Alain Destexhe

Self-sustained asynchronous irregular states and Up–Down states in thalamic, cortical and thalamocortical networks of nonlinear integrate-and-fire neurons

May 8, 2018(in press)

Abstract Randomly-connected networks of integrate-and-fire (IF) neurons are known to display asynchronous irregular (AI) activity states, which resemble the discharge activity recorded in the cerebral cortex of awake animals. However, it is not clear whether such activity states are specific to simple IF models, or if they also exist in networks where neurons are endowed with complex intrinsic properties similar to electrophysiological measurements. Here, we investigate the occurrence of AI states in networks of nonlinear IF neurons, such as the adaptive exponential IF (Brette-Gerstner-Izhikevich) model. This model can display intrinsic properties such as low-threshold spike (LTS), regular spiking (RS) or fast-spiking (FS). We successively investigate the oscillatory and AI dynamics of thalamic, cortical and thalamocortical networks using such models. AI states can be found in each case, sometimes with surprisingly small network size of the order of a few tens of neurons. We show that the presence of LTS neurons in cortex or in thalamus, explains the robust emergence of AI states for relatively small network sizes. Finally, we investigate the role of spike-frequency adaptation (SFA). In cortical networks with strong SFA in RS cells, the AI state is transient, but when SFA is reduced, AI states can be self-sustained for long times. In thalamocortical networks, AI states are found when the cortex is itself in an AI state, but with strong SFA, the thalamocortical network displays Up and Down state transitions, similar to intracellular recordings during slow-wave sleep or anesthesia. Self-sustained Up and Down states could also be generated by two-layer cortical networks with LTS cells. These models suggest that intrinsic properties such as adaptation and low-threshold bursting activity are crucial for the genesis and control of AI states in thalamocortical networks.

Integrative and Computational Neuroscience Unit (UNIC),
UPR2191, CNRS, Gif-sur-Yvette, France
E-mail: Destexhe@unic.cnrs-gif.fr

1 Introduction

In awake animals, the activity of single cortical neurons consist of seemingly noisy activity, with very irregular discharges at frequencies of 1-20 Hz and considerable fluctuations at the level of the membrane potential (V_m) (Matsumara et al., 1988; Steriade et al., 2001; Destexhe et al., 2003; Lee et al., 2006). Model networks of leaky integrate-and-fire (IF) neurons can display activity states similar to the irregular spike discharge seen in awake cortex. These so-called "asynchronous irregular" (AI) states contrast with the "synchronous regular" (SR) states, or with oscillatory states (Brunel, 2000). AI states have been observed more recently as a self-sustained activity in more realistic IF networks with conductance-based synapses (Vogels and Abbott, 2005). Such AI states typically require large network sizes, of the order of a few thousand neurons, to display characteristics consistent with experimental data (El Boustani et al., 2007; Kumar et al., 2008).

In reality, neurons do not behave as leaky IF models, but rather display complex intrinsic properties, such as adaptation or bursting, and these intrinsic properties may be important for neuronal function (Llinas, 1988). However, it is not clear to what extent AI states also appear in networks of more realistic neurons. Similarly, the genesis of AI states has never been investigated in the thalamocortical system. Recent efforts have been devoted to model intrinsic neuronal properties using variants of the IF model (Smith et al., 2000; Izhikevich, 2004; Brette and Gerstner, 2005). In the present paper, we use such models to analyze the genesis of AI states in cortical, thalamic and thalamocortical networks of neurons expressing complex intrinsic properties.

2 Methods

We successively describe the equations used for modeling neurons and synapses, the connectivity of the different

network models, as well as the methods used to quantify network activity.

2.1 Single-cell models

To capture the intrinsic properties of central neurons, such as the rebound bursting capabilities of thalamic cells and the spike-frequency adaptation in cortex, we considered the adaptive exponential IF (aeIF) model. This model consists of the two-variable IF model proposed by Izhikevich (2004), which was modified to include an exponential non-linearity around spike threshold, based on the exponential IF model of Fourcaud-Trocme et al. (2003). These two models were combined by Brette and Gerstner (2005), leading to the following set of equations:

$$C_m \frac{dV}{dt} = -g_L (V - E_L) + g_L \Delta \exp[(V - V_T)/\Delta] - w/S \quad (1)$$

$$\frac{dw}{dt} = \frac{1}{\tau_w} [a (V - E_L) - w],$$

where $C_m = 1 \ \mu F/cm^2$ is the specific membrane capacitance, $g_L = 0.05 \ mS/cm^2$ is the resting (leak) conductance, $E_L = -60$ mV is the resting potential (which is also equal to the reset value after spike), $\Delta = 2.5$ mV is the steepness of the exponential approach to threshold, $V_T = -50$ mV is the spike threshold, and $S = 20,000 \ \mu m^2$ is the membrane area. When V reaches threshold, a spike is emitted and V is instantaneously reset and clamped to the reset value during a refractory period of 2.5 ms. w is an adaptation variable, with time constant $\tau_w = 600$ ms, and the dynamics of adaptation is given by parameter a (in μS). At each spike, w is incremented by a value b (in nA), which regulates the strength of adaptation, as analyzed in more detail in the next section.

2.2 Single-cell intrinsic properties

The Brette-Gerstner-Izhikevich model was reported to display a wide range of intrinsic neuronal properties (Izhikevich, 2004; Brette and Gerstner, 2005). We focus here only on a few cell types commonly encountered in the thalamocortical system. Cortical neurons were modeled as "regular spiking" (RS) cells with spike-frequency adaptation (Connors and Gutnick, 1990), which corresponds to the parameters $a = 0.001 \ \mu S$ and $b = 0.04$ nA in the aeIF model (Fig. 1A). The strength of adaptation can be modulated by varying the parameter b, with $b = 0.005$ nA for weakly adapting cells (Fig. 1B). This parameter was estimated heuristically based on Hodgkin-Huxley type models and RS cells found in different preparations (Pospischil et al., 2008). For $b = 0$, the model generated responses with a negligible level of adaptation (Fig. 1C), similar to the "fast-spiking" (FS) cells encountered in cortex, and which corresponds mostly to cortical inhibitory neurons

(Connors and Gutnick, 1990). The latter will be used to model cortical inhibitory interneurons in the present model.
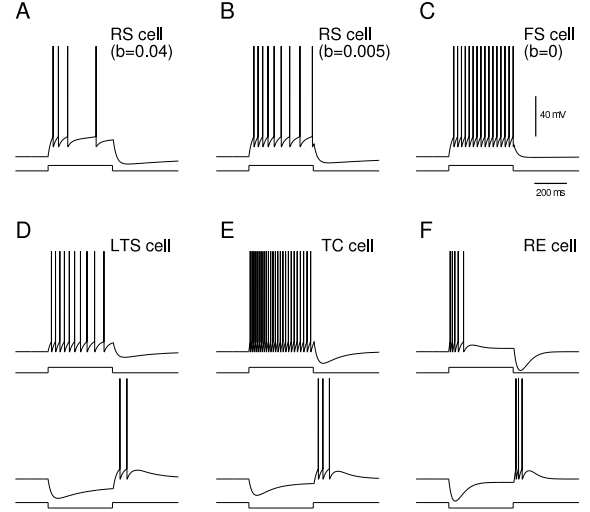
Fig. 1 Classes of neurons with different intrinsic neuronal properties as modeled by the adaptive exponential integrate-and-fire model. A. Regular-spiking (RS) neuron with strong adaptation. B. RS neuron with weak adaptation. C. Fast-spiking (FS) cell with negligible adaptation. D. Low-threshold spike (LTS) cell. E. Thalamocortical (TC) neuron. F. Thalamic reticular (RE) neuron. In all cases, the response to a depolarizing current pulse of 0.25 nA is shown on top. For D-F, the bottom curves show the response to a hyperpolarizing current pulse of -0.25 nA. The units of parameter b in A-C are nA.

Increasing the parameter a leads to bursting activity (Izhikevich, 2004). If we consider a moderate value of $a = 0.02 \ \mu S$, the model neuron also displays spike-frequency adaptation, even with $b = 0$ (Fig. 1D, top). However, this model also generates a rebound burst in response to hyperpolarizing pulses, while the conventional spike threshold is unchanged (Fig. 1D, bottom). This behavior is similar to the cortical low-threshold spike (LTS) cells (de la Peña and Geijo-Barrientos, 1996).

A further increase of parameter a leads to more robust bursting activity and weaker spike-frequency adaptation, producing patterns of responses with moderate adaptation and strong rebound bursts (Fig. 1E). This behavior was obtained for $a = 0.04 \ \mu S$ and $b = 0$. With larger values, $b = 0.08 \ \mu S$ and $a = 0.03$ nA, the model generated bursting activity in response to both depolarizing and hyperpolarizing stimuli (Fig. 1F), similar to thalamic reticular (RE) neurons (Destexhe and Sejnowski, 2003).

Similar intrinsic properties as well as other types of behavior could be generated by other combinations of parameters (see Izhikevich, 2004), but were not considered here.

2.3 Network models

Network models were constructed based on this aeIF model, according to the following equations:

$$C_m \frac{dV_i}{dt} = -g_L (V_i - E_L) + g_L \Delta_i \exp[(V - V_{Ti})/\Delta_i] - w_i/S$$
$$- \sum_j g_{ji} (V_i - E_j) \qquad (2)$$
$$\frac{dw_i}{dt} = \frac{1}{\tau_{w_i}} [a_i (V_i - E_L) - w_i],$$

where V_i is the membrane potential of neuron i, and all parameters are as in Eqs. 1, but were indexed to allow variations according to cell type (see Results). The term $\sum_j g_{ji} (V_i - E_j)$ accounts for synaptic interactions, where g_{ji} is the conductance of the synapse from neuron j to neuron i (and which can be zero), and E_J is the reversal potential of the synapse ($E_j = 0$ mV for excitatory synapses and -80 mV for inhibitory synapses). Synaptic conductance time courses were exponential; once the presynaptic cell fired, a fixed increment was assigned to the corresponding g_{ji} (g_e and g_i for excitatory and inhibitory synapses, respectively), after which g_{ji} decays exponentially with a fixed time constant (5 ms for excitation and 10 ms for inhibition). Different synaptic strengths g_e and g_i were considered depending on the network type (see Results). No synaptic delays were considered.

Note that because only small networks are considered here (of the order of tens to a few thousand neurons), synaptic strengths need necessarily to be large compared to physiological values. Typical values are $g_e = 6$ nS and $g_i = 67$ nS (Vogels and Abbott, 2005), which correspond to postsynaptic potential sizes of 11 mV and 8.5 mV, respectively, at -70 mV and at rest. The amplitude of postsynaptic potentials will be vastly different in an active network, with typical values around 0.5 mV, respectively (El Boustani et al., 2007). Such a large difference is of course a property only seen in conductance-based models. It was shown that large networks (10,000 to over 100,000 neurons), with large numbers of synapses per neuron (> 500), are necessary to achieve configurations with plausible synaptic conductance values (El Boustani et al, 2007; Kumar et al., 2008).

To initiate activity, a number of randomly-chosen neurons (from 2% to 10% of the network) were stimulated by random excitatory inputs during the first 50 ms of the simulation. The mean frequency of this random activity was high enough (200-400 Hz) to evoke random firing in the recipient neurons. In cases where self-sustained activity appeared to be unstable, different parameters of this initial stimulation were tested. It is important to note that after this initial period of 50 ms, no input was given to the network and thus the activity states described here are self-sustained with no external input or added noise. The only source of noise was the random connectivity (also termed "quenched noise".)

All equations were solved using the NEURON simulation environment (Hines and Carnevale, 1997).

2.4 Connectivity

In all cases, the connectivity was random, but respected the anatomical and morphological constraints about the connection probability between the different cell types, as described below for thalamus, cortex and thalamocortical relations.

2.4.1 Thalamus

The structure of the thalamus was approximated by a two layer network of randomly connected cells, including one layer of thalamocortical (TC) relay cells and one layer of thalamic reticular (RE) cells. In a number of species such as rodents, some thalamic nuclei are devoid of interneurons (Jones, 1985). There is also evidence that thalamic interneurons do not play a major role in the genesis of internal dynamics, for example in oscillations (Steriade et al., 1985; von Krosigk et al., 1993). Thus, thalamic interneurons were not incorporated for simplicity. The thalamic network had 10 times less neurons compared to the cortical network, which corresponds to morphological estimates (Sherman and Guillery, 2001). Based on anatomical data showing that axonal projections within the thalamic circuitry are local but sparse (FitzGibbon et al., 1995; Jones, 1985; Minderhoud, 1971), the excitatory projection from TC to RE cells had a connection probability of 2%, as in cortex, while the RE to TC inhibitory projection was more dense (Kim et al., 1997), and was here of a probability of about 8%. The same density was assumed from inhibitory connections between RE cells.

This connectivity scheme corresponds to thalamic networks of size N=100. When comparing networks of different size, the connection probability was rescaled inversely to network size, such that the number of synapses received by the neurons was invariant to size.

2.4.2 Cortex

In area 5 of cat cerebral cortex, axon collaterals from pyramidal cells are profuse and dense but remain localized within a few hundreds of microns (Avendaño et al., 1988). The connection densities of cells in the cortical network were organized such that each pyramidal cell (PY) or interneuron (IN) projected to a small proportion of about 2% of the size of the network. The same connection probability was also assumed for inhibitory connections. This connectivity was the same as that assumed in a previous model

of cortical AI states (Vogels and Abbott, 2005). These connection probabilities correspond to a cortical network of N=2000 neurons. As for thalamic networks, when different cortical network size were compared, the connection probability was rescaled inversely to network size to preserve the number of connections per neuron.

2.4.3 Thalamocortical relations

The thalamocortical and corticothalamic connections were also random, and their densities were estimated from morphological studies as follows. Ascending thalamocortical fibers give most of their synaptic contacts in layers I, IV and VI of cerebral cortex (White, 1986). Given that layer VI pyramidal neurons constitute the major source of corticothalamic fibers, these cells therefore mediate a monosynaptic excitatory feedback loop (thalamus-cortex-thalamus; White and Hersch, 1982), which was modeled here. This monosynaptic loop is also demonstrated by thalamically-evoked antidromic and monosynaptic responses in the same, deeply lying cortical cell (see Fig. 5 in Steriade et al., 1993b). The model incorporated the fact that all thalamic-projecting layer VI pyramidal cells connect TC cells while leaving axon collaterals in the RE nucleus. However, lower layer V pyramids also project to thalamic nuclei, but they do not leave collaterals in the RE nucleus (Bourassa and Deschênes, 1995); the latter were not modeled. We did not include either the influence of some thalamic intralaminar nuclei that project diffusely to the cerebral cortex as well as receive projections from it (Jones, 1985).

Projections between thalamus and cortex are also local and sparse (Avendaño et al., 1985; Jones, 1985; Robertson and Cunningham, 1981; Updyke, 1981) but have more divergence than intrathalamic or intracortical connections (Bourassa and Deschênes, 1995; Freund et al., 1989; Landry and Deschênes, 1981; Rausell and Jones, 1995). In the model, each PY cell had some probability of connecting to TC and RE cells, but due to the large number of cortical neurons, this corticothalamic connectivity was much more extended than local thalamic connectivity, so that cortical synapses were majoritary in thalamus (80% of synapses in TC cells were from cortex), as demonstrated experimentally (Sherman and Guillery, 2001). Similarly, each TC cell projected to PY and IN cells, using a connection probability of 2%. In these conditions, cortical connectivity was still dominated by intracortical synapses, as only about 6% of excitatory synapses were from thalamus, which corresponds well to estimates from morphological estimates (Braitenberg and Shutz, 1998).

Thus, similar to a previous model (Destexhe et al., 1998), this thalamocortical model can be thought of representing cerebral cortex Layer VI, connected reciprocally with its corresponding thalamic area. All axonal projections of a given type were identical in extent from cell to cell and all synaptic conductances were equal. The total synaptic conductance on each neuron was the same for cells of the

same type, independently of the size of the network. The connection probabilities are summarized in Table 1.

Connection type	Connection probability	Nb. synapses / neuron
PY $\rightarrow$ PY	2 %	32
PY $\rightarrow$ IN	2 %	32
IN $\rightarrow$ PY	2 %	8
IN $\rightarrow$ IN	2 %	8
PY $\rightarrow$ TC	2 %	32
PY $\rightarrow$ RE	2 %	32
TC $\rightarrow$ RE	2 %	2
RE $\rightarrow$ TC	8 %	8
RE $\rightarrow$ RE	8 %	8

Table 1 Connection probabilities between the different cell types. The probability is calculated for *outgoing* synapses, for example for the TC $\rightarrow$ RE connection, the number indicated is the probability that a given TC cell connects one RE cell. In the last column, an example of the average number of *incoming* synapses (afferent synapses per neuron) is indicated for each type of connection in a network with 1600 PY, 400 IN, 100 TC and 100 RE neurons (TC = thalamocortical neurons; RE = thalamic reticular neurons; PY = cortical excitatory neurons; IN = cortical inhibitory interneurons).

2.4.4 Two-layer cortical model

Interlayer connectivity in cerebral cortex involves both excitatory and inhibitory connections, but is predominantly excitatory, with a connection density specific to the layers considered (Thomson and Bannister, 2003; Binzegger et al., 2004). Interlayer (vertical) connectivity is also in general less dense than intra-layer (horizontal) connections. Two layers of cortical networks were modeled as described above, with excitatory-only interlayer connectivity with a probability of 1%, which is twice less dense than intra-layer connectivity (2%; see Table 1).

2.5 Quantification of network states

Network states were quantified according to two aspects: regularity and synchrony. To quantify the degree of temporal regularity, we used the coefficient of variation (CV) of the interspike intervals (ISI), averaged over all cells the network:

$$CV_{ISI} = \left\langle \frac{\sigma_i^{ISI}}{\overline{ISI}_i} \right\rangle , \qquad (3)$$

where the brackets $\langle \rangle$ indicate an average over all neurons, while $\overline{ISI}_i$ and σ_i^{ISI} are respectively the mean and standard deviation of the ISIs of neuron i. The CV_{ISI} is expected to take large values ≥ 1 for temporally irregular systems (the CV is 1 for a Poisson process). In this paper, we considered that a system is "irregular" if the CV_{ISI} exceeds a value of 1.

The degree of synchrony was quantified using the averaged pairwise cross-correlation between neurons in the network:

$$CC = \left\langle \frac{Cov(S_i, S_j)}{\sigma(S_i)\sigma(S_j)} \right\rangle , \qquad (4)$$
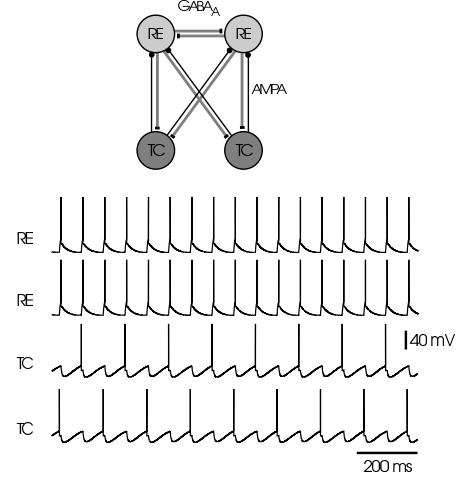
where the brackets $\langle \rangle$ indicate an average over a large number of disjoint pairs of neurons (in general 500 pairs were used), $Cov(S_i, S_j)$ is the covariance between two spike counts S_i, S_j, and $\sigma(S_{i,j})$ is the standard deviation of each spike count. Spike counts were computed by counting spikes in successive time bins of fixed duration (5 ms; all results were also checked using 2 ms). The CC is comprised between -1 and 1, and takes high values only for synchronous states. A given network state can reasonably be considered as "asynchronous" if CC is low enough (typically < 0.1). These criteria and methods were similar to that used previously to characterize different states in network models (Brunel, 2000; Kumar et al., 2008; El Boustani and Destexhe, 2009).

Fig. 2 Oscillatory behavior in simple circuits of thalamic neurons. Top scheme: minimal circuit for spindle oscillations, consisting of two TC and two RE cells interconnected with excitatory (AMPA) and inhibitory (GABA$_A$) synapses as indicated. This circuit generated oscillations at a frequency around 12 Hz, and in which RE cells fired at every cycle while TC cell fired sub-harmonically, once every two cycles. Synaptic conductance values: $g_e = 30$ nS, $g_i = 30$ nS

3 Results

We successively consider network models for thalamus, cortex and the thalamocortical system, and analyze their dynamics as a function of their size and intrinsic properties.
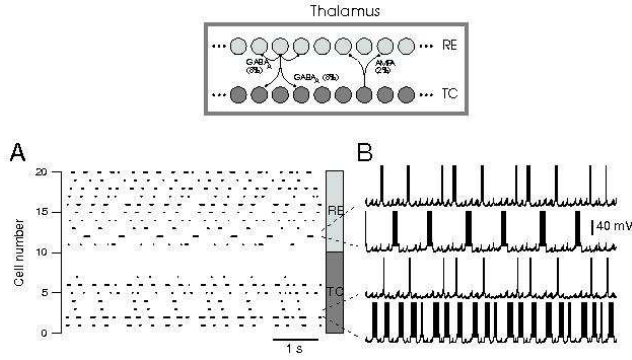
3.1 Networks of thalamic neurons

Interconnected thalamic TC and RE cells can generate oscillations in the spindle (7-14 Hz) frequency range (reviewed in Destexhe and Sejnowski, 2003). We first verified that the aeIF models outlined above were capable of replicating this oscillatory behavior. A small circuit of interconnected TC and RE cells was built, where all cells were interconnected, except for TC cells which do not have interconnections (Fig. 2, scheme). As shown in Fig. 2, this circuit generated self-sustained oscillations at a frequency around 10 Hz, with RE cells firing in response to EPSPs from TC cells, and TC cells firing in rebound to IPSPs from RE cells; the TC cells also generated subharmonic firing. These features are typical of spindle oscillations (Steriade, 2003). This behavior is only possible by taking into account the intrinsic properties of thalamic cells, and in particular the rebound bursting properties of TC cells (Destexhe and Sejnowski, 2003). As in more complex models, the oscillation frequency was dependent on the decay kinetics of synaptic currents, and the oscillation was observed for a large range of synaptic weights provided they were strong enough (not shown).

Small-size networks of TC and RE cells were considered by considering more diffuse and random connectivity between the two TC and RE layers, and weaker synaptic weights (see scheme in Fig. 3). In these conditions, a N=20 network (10 TC and 10 RE cells) generated oscillatory behavior, but in contrast to the small circuit considered above, these oscillations appeared to be aperiodic, as seen from both rasterplot and single cells in Fig. 3. A phase plot between two TC cells (Fig. 3B, inset), as well as the high value of the coefficient of variation ($CV_{ISI} = 1.36$ in this case), confirmed the aperiodic character of the oscillation. The raster plot also shows that there is little synchrony in the firing of TC or RE cells, unlike the circuit of Fig. 2. This was confirmed by the low value of the averaged cross-correlation ($CC = 0.025$). This state resembles the "asynchronous regular" states described earlier (Brunel, 2000). This behavior was robust to long integration times (up to 100 sec were tested) without evidence for periodic behavior, suggesting that this type of dynamics is self-sustained and aperiodic. Note that there is a possibility that these regimes are periodic, but with a very long period which grows exponentially with network size (Cessac, 2008; Cessac and Viéville, 2009; see also Crutchfield and Kaneko, 1988; Tél and Lai, 2008).

Networks comprising more thalamic neurons were considered based on a similar connectivity scheme and the same synaptic weights as for N=20. By increasing the size from N=40 to N=100 generated patterns of aperiodic oscillatory activity (Fig. 4). With larger sizes, the activity became more and more similar to an "asynchronous irregular" state. For example, for a N=100 network (Fig. 4C), the irregularity was high ($CV_{ISI} = 1.47$) and the synchrony was low ($CC = 0.016$).

Fig. 3 Irregular oscillatory activity states in networks of 20 randomly-connected thalamic neurons. Top: scheme of connectivity between the two layers of TC and RE cells, which were randomly connected. A. Raster plot of the spiking activity of the 20 neurons. B. V_m activity of two cells of each type. Synaptic conductance values: $g_e = 6$ nS, $g_i = 67$ nS. The connection probability was of 8 % (from RE to TC, and RE to RE) and 2% (from TC to RE), as in Table 1. The activity is shown after a transient time of 50 sec. Inset in B: phase plot of the V_m activity of cell 1 against that of cell 2, showing the non-periodic character of this activity (the CV_{ISI} was of 1.36 and the CC was of 0.025).
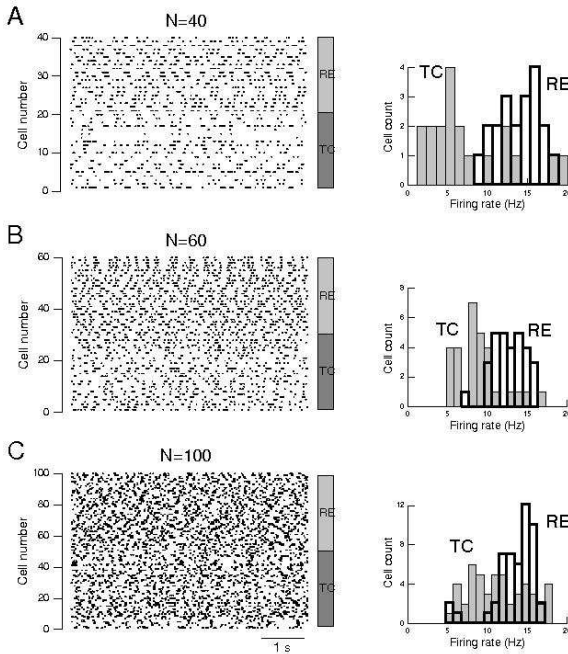
Fig. 4 Irregular activity states in thalamic networks of various sizes. The same connectivity scheme was used as in Fig. 3, but with larger sizes as indicated. Same synaptic conductance values and connection probabilities as in Fig. 3. *Left panels:* activity after a transient time of 50 sec. The CV_{ISI} and CC were respectively of 1.45 and 0.027 for N=40, 1.35 and 0.02 for N=60, and 1.47 and 0.016 for N=100. *Right panels:* distribution of firing rates for the two cell types.

This behavior was seen for a large domain of values for the synaptic conductances. This aspect, and more generally the robustness of irregular oscillations to synaptic conductances, was quantified in more detail in Fig. 5. The domain of oscillatory behavior was relatively large, provided both conductances were above some threshold value (about 4 nS for excitatory conductance inputs and 40 nS

for inhibitory conductances). The firing rate tended to increase with the level of inhibition, which is presumably a consequence of the rebound properties of thalamic neurons. There were also small differences between N=20 and N=100 networks: the mean firing rate tended to be larger for $N = 100$, while the averaged pairwise correlation was lower (Fig. 5, bottom panels).
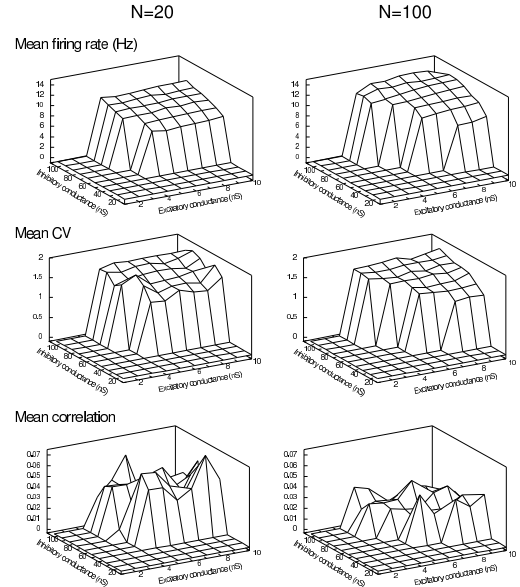

Fig. 5 Domain of conductance parameters for self-sustained irregular states in thalamic networks. *Top Panels:* mean activity rate calculated over the entire network, shown as a function of the synaptic conductance values (g_e for excitation and g_i for inhibition) for N=20 (left) and N=100 (right). *Middle panels: corresponding coefficients of variation CV_{ISI} calculated over all cells. Bottom panels: corresponding mean pairwise correlation CC calculated over $N/2$ disjoint cell pairs in each network.* The irregular oscillations appeared within a domain limited approximately by $g_e > 4$ nS and $g_i > 40$ nS. Transient oscillations that did not survive 10 sec simulation time are not indicated.

3.2 Cortical networks

We next considered the activity of cortical networks composed of excitatory RS and inhibitory FS cells, randomly connected. Unlike thalamic networks, cortical circuits of this type do not generate self-sustained AI states unless large networks are considered (Vogels and Abbott, 2005; Kumar et al., 2008). Compared to previous studies using leaky IF models, the present model considers more complex IF models, in particular for RS cells which display prominent spike-frequency adaptation. The cortical network had 80% excitatory and 20% inhibitory cells, and was randomly connected (see scheme in Fig. 6). In these conditions, the genesis of self-sustained AI states was possible, but was highly dependent on the level of adaptation, as illustrated in Fig. 6. For strong to moderate adaptation, the network generated AI states but they were transient

and did not survive more than a few seconds (Fig. 6A). For weak adaptation, the AI states could be sustained (Fig. 6B).
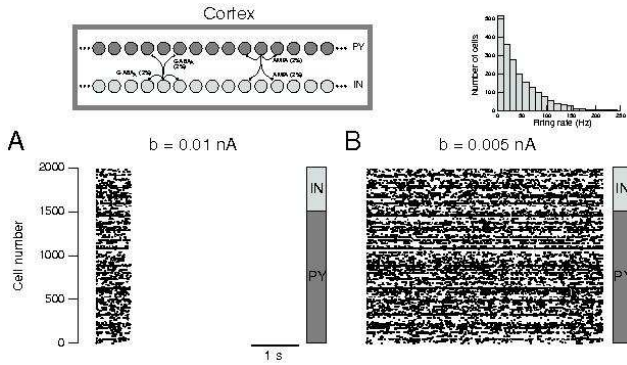

Fig. 6 Transient and self-sustained irregular states in randomly-connected networks of cortical neurons. Top: scheme of connectivity. A. Transient AI state in a N=2000 network, when the RS neurons had a significant adaptation. B. Self-sustained AI state in the same network after diminishing the strength of adaptation (CV_{ISI} = 2.47, CC = 0.005; Inset: distribution of firing rates). Synaptic conductances: g_e = 6 nS, g_i = 67 nS, and connection probability as in Table 1. Note that in this case, PY cells are all of RS type, while all IN cells are of FS type.

The situation was radically different in the presence of LTS cells. Networks of relatively small size, N=400 (Fig. 7A) or N=500 (Fig. 7B), could generate self-sustained AI states if a proportion of LTS cells was present (LTS cells were connected identically as for RS cells). For N=400, the system exhibited intermittent-like dynamics (Fig. 7A), which was typical of the transition between self-sustained oscillations, and AI type behavior. In this intermittency, the network switches between SR and AI states, while for larger networks, the dynamics remain in the AI state without intermittency (Fig. 7B).

To further characterize the role of LTS cells, the cross-correlation between LTS cells and inhibitory FS cells was calculated and compared with the cross-correlation between RS and RS cells (Fig. 8). Because the firing FS cells leads only to inhibition of RS cells, the cross-correlation is negative for positive values of the time lag (Fig. 8, arrow in black curve). It is also negative for negative time lags, presumably due to the inhibition between FS cells. However, when correlating LTS cells with FS cells, the pattern was different for positive time lags, and positive correlations appeared (Fig. 8, arrow in red curve). This indicates that FS cells tend to excite LTS cells after some delay of about 70 ms, which seems to correspond to the post-inhibitory rebound because LTS and RS cells had the same connectivity. This positive value was also observed for other network configurations with LTS cells (not shown).

These results suggest that, through their post-inhibitory rebound property, the presence of LTS cells increases the excitability of the network, enabling the genesis of AI states with relatively small network sizes. Indeed, by simulating different network size, with and without LTS cells, re-
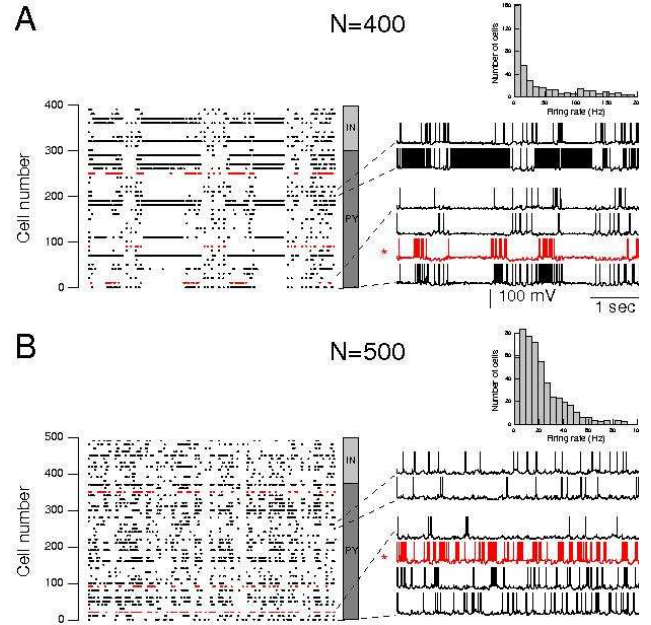

Fig. 7 Self-sustained irregular states in small cortical networks with LTS cells. The network was composed of 80% excitatory (PY) cells and 20% inhibitory (IN) cells. 95% of PY cells were RS type and 5% were of LTS type, while all IN cells were of FS type. A. N=400 network displaying self-sustained irregular activity (CV_{ISI} = 2.84, CC = 0.05). B. AI state in a N=500 network (CV_{ISI} = 2.07, CC = 0.05). In each case, the raster is shown on the left, with a few example cells on the right, together with the firing rate distribution in insets. Same synaptic conductances and connection probabilities as in Fig. 6. LTS cells are indicated in red (*).
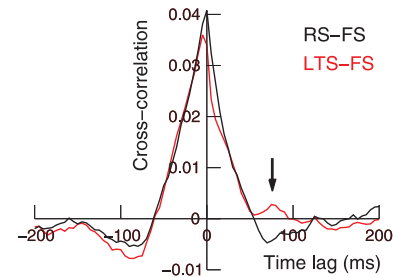
Fig. 8 Sign of rebound activity in LTS cells from cross-correlations. Cross-correlations between RS and FS cells (black), as well as between LTS and FS cells (red) were computed from a N = 500 network (same simulation as in Fig. 7B, but with a total time of 50 sec). The cross-correlations were calculated from instantaneous rates (spiking activity in successive 5 ms bins), and were averaged between 400 non-overlapping pairs of cells for each type. The arrow shows that around 70 ms, a positive peak appears for LTS-FS correlations, presumably due to the post-inhibitory rebound of LTS cells. As expected, all correlations peaked at negative delays, betraying the excitatory action of RS and LTS cells onto FS cells.

vealed that the minimal size needed to sustain AI states was highly reduced in the presence of LTS cells (Fig. 9). Moreover, the minimal size was inversely related to the proportion of LTS cells (from 0% to 20%; see Fig. 9).
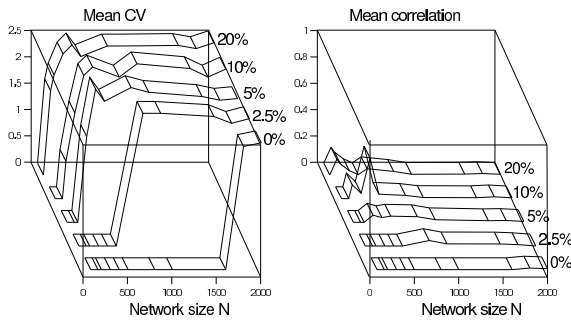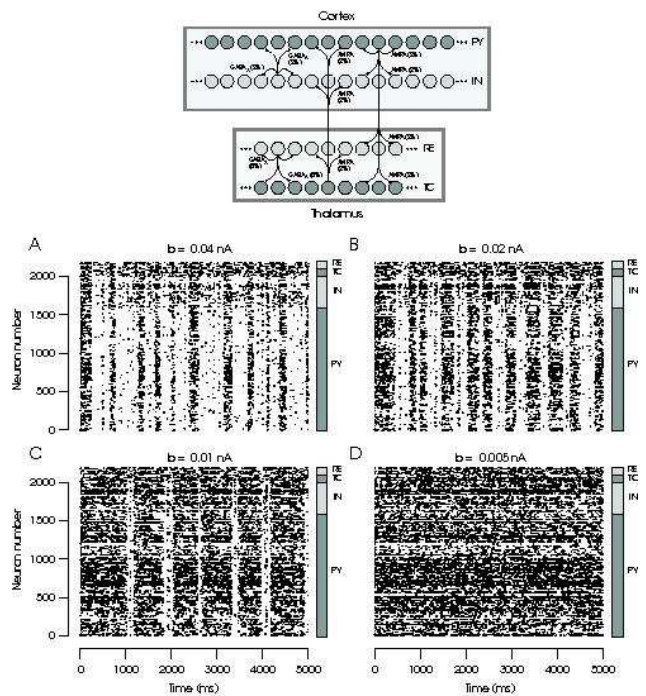
Fig. 9 Minimal size for sustaining irregular states in cortical networks. Simulations similar to Fig. 7 were performed for different network sizes (from 80 to 2000 neurons), and for different proportions of LTS cells (from 020correlation coefficient (*CC*, right) are plotted as a function of network size and proportion of LTS cells. All self-sustained states had high *CV* and low *CC*, as indicated (*CV_ISI* = 0 and *CC* = 0 indicate states with no self-sustained activity. The minimal size for displaying AI states was much reduced if LTS cells were present. It was of 1800, 800, 300, 200 and 100 neurons, respectively for 0, 2.5, 5, 10 and 20% of LTS cells.


Fig. 10 Self-sustained irregular and Up/Down states in thalamocortical networks. Top: Scheme of connectivity of the thalamocortical network. The network had 4 layers of cortical pyramidal (PY), cortical interneurons (IN), thalamic reticular (RE) and thalamocortical (TC) relay cells. Each cell is represented by a filled circle (dark gray = excitatory cells; light gray = inhibitory cells), and synaptic connections are schematized by arrows. Bottom panels: From A to D, the same model was used (2200 cells total, 1600 PY, 400 IN, 100 TC and 100 RE cells), but with different strengths of adaptation (from b=0.04 nA in A to b=0.005 nA in D). In all rasters, only 10% of cells are shown for each cell type, and the 4 layers of cells are indicated on the right. For the AI state in D, cortical neurons were characterized by a mean firing rate of 44 Hz, a coefficient of variation of CV_{ISI} = 2.45 and a pairwise correlation of CC = 0.004.

3.3 Thalamocortical networks

The behavior of a thalamocortical network connected as schematized in Fig. 10 (top) also depends on the level of adaptation in cortical cells. With strong adaptation, the network displayed alternating dynamics of active and silent periods (Up/Down states; see Fig. 10A). Progressively diminishing adaptation (Fig. 10B-C) led to dynamics where the silent periods (Down states) were diminished while the active (Up) states were longer. For weak adaptation, the network displayed self-sustained AI states with no silent period (continuous Up state; Fig. 10D). This latter state qualifies as an AI state, with CV_{ISI} = 2.45 and CC = 0.004. The corresponding cellular activities are shown in Fig. 11. Note that the firing rate of the model (around 40 Hz on average) is larger than experimental data, for both up states and AI states. This is due to the relatively small size of the network, as only networks of large size can self-sustain AI states at low rates (El Boustani and Destexhe, 2009).

Because neuromodulatory substances, such as acetylcholine or noradrenaline, block the K$^+$ conductances responsible for adaptation (McCormick, 1992), the transition from Up & Down states to self-sustained active states in Fig. 10 by reducing spike-frequency adaptation reminds the brain activation process. Experimentally, a transition from Up/Down state dynamics to self-sustained activated states can be obtained by electrical stimulation of the brain stem, inducing a cascade of cholinergic actions in thalamus and cortex (Fig. 12A; Steriade et al., 1993a; Rudolph et al., 2005). One of the most prominent of these actions is a reduction in spike-frequency adaptation (McCormick, 1992). A very similar transition can be obtained in the model when the adaptation is reduced (from b=0.02 nA in A to b=0.005 nA; see Fig. 12B).

3.4 Two-layer cortical networks

The above mechanism for Up/Down states relies on the fact that the thalamus displays self-sustained AI states. In the present section, we present a similar mechanism but internal to cortex, in better agreement with experiments which reported self-sustained Up/Down state dynamics in cortical slices (Sanchez-Vives and McCormick, 2000; Cossart et al., 2003). To this end, the results from preceding sections were combined into a "two layer" cortical network in which one layer consisted of RS and FS cells, as described above (Fig. 6A), while a second layer was a smaller network of RS and FS cells, with some proportion of LTS cells, as in Fig. 7B. These two networks were referred as "Layer A" and "Layer B", respectively (see scheme in Fig. 13). When reciprocally connected with excitatory synapses, this 2-layer system exhibited Up/Down state dynamics with a mechanism similar to that described in the preceding section for thalamocortical networks. In the present case, the Layer B network generated self-sustained activity, which served to ignite activity in the Layer A (see raster in Fig. 13, bottom). Interestingly,
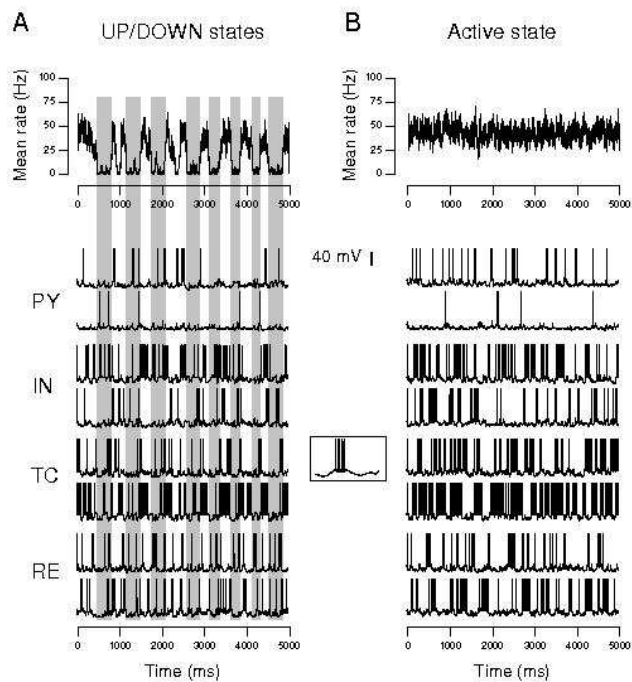
Fig. 11 Cellular and averaged activity during self-sustained states in thalamocortical networks. The top graphs indicate the instantaneous mean spike rate of cortical cells (in successive 1 ms bins), while the bottom traces display the V_m activity of two cells of each type as indicated. A. Up/Down state transitions (same simulation as in Fig. 10B). The largest Down states are indicated in gray. B. Sustained active state (same simulation as in Fig. 10D). The same cells are indicated for each simulation. The inset shows a rebound burst in a TC cell at 10 times higher temporal resolution.

this simulation shows that a network displaying transient dynamics (Fig. 6A) connected with a network displaying AI states (Fig. 7B) yields a system displaying a different type of activity, Up and Down states in this case. This dynamics was entirely self-sustained and coexisted with a stable resting state (Fig. 13, arrow). All of these behaviors are indissociable from the particular intrinsic properties of the neurons present in the system.

4 Discussion

In this paper, we have shown that networks of neurons displaying complex intrinsic properties can display various type of AI states. The main finding were that (a) thalamic networks, where neurons are endowed with rebound bursting capabilities, can display AI states for remarkably small size (N∼100). (b) Cortical networks display AI states, as reported previously (Brunel 2000, Vogels and Abbott, 2005), but when adaptation is included in excitatory neurons, cortical networks generate AI states only for weak adaptation. (c) Including a small proportion of LTS cells in cortical networks greatly reduces the minimal size needed to generate AI states. (d) thalamocortical networks can display AI states or Up/Down state dynamics, depending on the level of adaptation in cortical cells. (e) Two-layer cortical
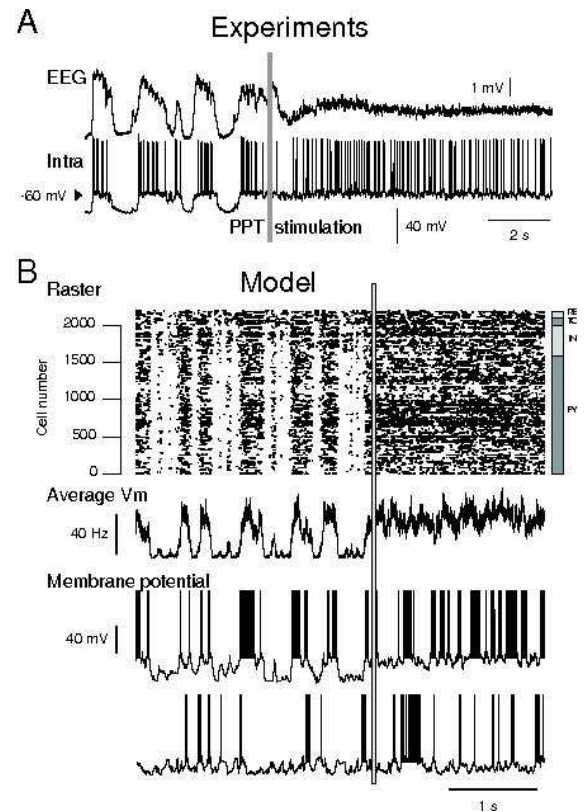

Fig. 12 Experiments and model of the transition from Up/Down to activated states. A. Transition from Up/Down state dynamics to an activated state, evoked by stimulation of the pedonculo-pontine tegmentum (PPT) in an anesthetized cat. The two traces respectively show the EEG and intracellular activity recorded in parietal cortex. B. Similar transition obtained by changing the value of *b* from 0.02 nA to 0.005 nA (gray line). All other parameters were identical to Fig. 10. Panel A modified from Rudolph et al., 2005.

networks can self-sustain Up/Down states solely from intrinsic dynamics.

These numerical observations suggest that spike-frequency adaptation acts against the genesis of AI states, and tends to silence the network (Fig. 6). Adaptation diminishes excitability, and several neuromodulators increase cortical excitability by blocking the slow K^+ conductances responsible for adaptation (McCormick, 1992). Neuromodulation has also strong effects on leak conductances, in particular in the thalamus (McCormick, 1992). We did not attempt to incorporate such effects in this model, but the precise modeling of neuromodulation, and possible transitions from AI to various types of oscillatory behavior, constitutes a possible extension of the model.

The presence of LTS neurons tends to greatly favor AI states. This is consistent with the genesis of AI states in very small thalamic networks (N∼100; Fig. 4), where all neurons display LTS. In cortex, inclusion of a small proportion of LTS cells (as observed experimentally; see de la Pena and Geijo-Barrientos, 1996; Destexhe et al., 2001), greatly reduces the minimal size to display AI states. The probable mechanisms is that LTS cells renders the network
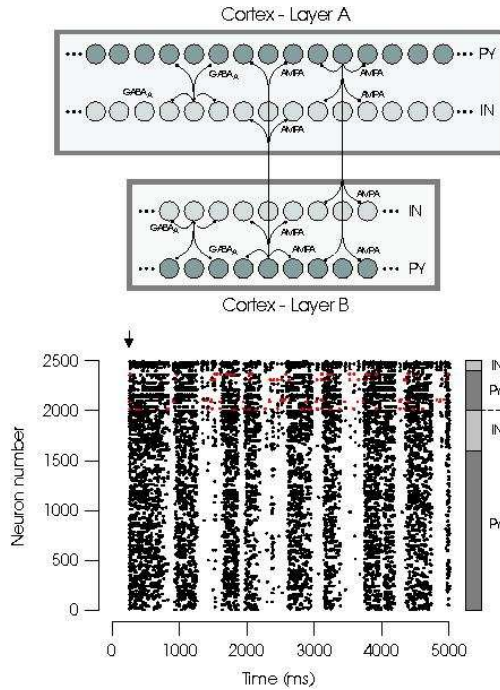
Fig. 13 Up/Down state dynamics in a 2-layer cortex model with LTS cells. *Top:* Scheme of connectivity between two networks of N=2000 (Layer A) and N=500 (Layer B) neurons. Layer B had 10% LTS cells and was capable of displaying self-sustained AI states. *Bottom:* Raster of the activity during 5 seconds (LTS cells shown in red). The stimulation of the network started at t=250 ms (arrow), and switched the stable resting state to self-sustained Up/Down state dynamics (CV_{ISI} = 2.49, CC = 0.069). Parameters for the Layer A network were identical to Fig. 6A, and Layer B was identical as Fig. 7B, with 10% of LTS cells. The interlayer connectivity was only excitatory and had a connection probability of 1%.

insensitive to "gaps" of firing, caused by occasional synchronized inhibition, and which usually stops the activity. These gaps are followed by rebound bursts in a minority of LTS cells if they are present, and thus renders the network less vulnerable to such gaps. This also suggests that LTS cells could be indicative of networks that generate AI type of activity. It would be interesting to investigate in more detail, and perhaps theoretically, the contrasting effects of adaptation and LTS on the genesis of AI states. Inclusion of other types of bursting cells, such as intrinsically bursting neurons (Connors and Gutnick, 1990) or inhibitory LTS cells (Xiang et al., 1998), also constitutes a possible extension of this study.

In the thalamocortical system, the association of thalamic networks and cortical networks generates a variety of states, including AI states and different forms of Up/Down state dynamics, for different levels of adaptation in cortical excitatory cells. Reducing adaptation, mimicking the action of some neuromodulators such as acetylcholine, may induce a transition from Up/Down state dynamics to sustained AI states. This transition is similar to the activation of the brain by neuromodulators, which also can produce a transition between slow-wave activity with Up/Down state dynamics, to the so-called "desynchronized" EEG activity. This transition naturally occurs upon awakening from

slow-wave sleep (Steriade, 2003), or can be induced by stimulation of the ascending neuromodulatory systems (Steriade et al, 1993a; Fig. 12A), and can be mimicked by the thalamocortical model by a reduction of the adaptation parameter b (Fig. 12B). This is consistent with the action of neuromodulators, such as acetylcholine, to block or reduce K^+ conductances responsible for spike-frequency adaptation (McCormick, 1992).

In this paper, there was no attempt to reproduce the correct cellular conductance patterns of the different network states. Experimental measurements show that the input resistance of cortical neurons *in vivo* is reduced by 3 to 5 times compared to quiescent states, in both anesthetized animals (Contreras et al., 1996; Borg-Graham et al., 1998; Pare et al., 1998; Destexhe and Pare, 1999) and awake animals (Baranyi et al., 1993a, 1993b; Steriade et al., 2001; reviewed in Destexhe et al., 2003; Destexhe, 2007). The excitatory and inhibitory synaptic conductances were also measured in anesthetized (Borg-Graham et al., 1998; Rudolph et al., 2005) and awake preparations (Rudolph et al., 2007). Reproducing the correct conductance state in individual neurons requires large network sizes (El Boustani et al., 2007; Kumar et al., 2008), and was not attempted here. We rather focused on the minimal size necessary to obtain AI states in different network configurations, but obtaining states fully consistent with experimental data will require substantial computational resources to simulate large networks of aeIF neurons, and constitutes a logical follow-up of this study.

It is also interesting to note that this thalamocortical model is different than previous models of Up/Down states in cortical networks (Timofeev et al., 2000; Compte et al., 2003; Parga and Abbott, 2007). Previous models have considered additional mechanisms to initiate Up states, which amounts to have some cortical neurons spontaneously firing or external noise. In contrast, Up/Down state dynamics arise here entirely from self-sustained activity. In the thalamocortical model, the cortex is in a state generating transient dynamics (as in Fig. 6A), while the thalamus is in an AI state. The system generates a transient Up state, then the activity stops, leading to a Down state. The activity restarts due to the firing of TC cells which triggers a new Up state, and the cycle restarts. This model therefore does not generate Up/Down state dynamics in the cortex alone, contrary to observations of Up/Down states in cortical slices (Sanchez-Vives and McCormick, 2000; Cossart et al., 2003) or in cortical organotypic cultures (Plenz and Aertsen, 1996). It nevertheless accounts for the fact that the thalamus ignites the Up states in the intact thalamocortical system *in vivo* (Contreras and Steriade, 1995; Grenier et al., 1998).

Similar Up/Down state dynamics were also observed in a more sophisticated model of the cortex allowing layered connectivity, in which a small sub-network played the role of AI state generator, while the rest of the network was passive and generated transient dynamics, as in Fig. 6A. The interconnections between two such net-

works generated Up/Down state dynamics very similar to the thalamocortical model, except that in this case, the activity was entirely generated within the cortex, in agreement with cortical slice experiments. The sub-network displaying self-sustained AI states (Layer B in Fig. 13) may represent Layer V networks, which were reported to initiate the activity during Up states in cortical slices (Sanchez-Vives and McCormick, 2000). Also similar to the thalamocortical model, this two-layer model of the cortex generated Up/Down state dynamics entirely from the internal dynamics of the system, without the requirement of spontaneously firing cells, or additional noise, as in previous models. The bistability of this system was illustrated by the coexistence of a stable resting state and Up/Down state dynamics (Fig. 13, arrow). Note that here, the specific choice of networks with LTS cells (layer B) should not be considered as a prediction, as similar dynamics should also be observed if Layer B was a network of RS and FS cells displaying AI states (as in Fig. 6B). The essential prediction here is that a network with self-sustained activity, combined with another network displaying spike-frequency adaptation, is a possible generator of self-sustained Up/Down state dynamics.

Finally, the present model reports a variety of AI states in different network configurations, but it is important to note that AI states may be transient in nature. Transient chaotic regimes have been extensively studied (Crutchfield and Kaneko, 1988; Zillmer et al., 2006; Cessac, 2008; Cessac and Viéville, 2009; reviewed in Tél and Lai, 2008). The lifetime of these transient regimes is known to increase exponentially with network size (Crutchfield and Kaneko, 1988; Kumar et al., 2008; Tél and Lai, 2008; El Boustani and Destexhe, 2009). For large networks, of the order of thousand or more neurons, this lifetime can reach considerable times (beyond any reasonable simulation time; see Kumar et al., 2008). It is thus difficult to formally establish the transient nature of such states with numerical simulations. However, although AI states may not represent a stable attractor of the system, they are nevertheless relevant because they represent the dynamics of the system within any reasonably accessible time period.

In conclusion, we have shown here what should be considered as the beginning of an exploration of the collective dynamics of populations of neurons endowed with complex intrinsic properties as given by the aeIF model. The presence of such properties has important effects on network behavior, and in particular affects the genesis of AI state. AI states are not possible in small networks without LTS properties, which certainly constitutes an interesting prediction. More generally, future studies should investigate intrinsic properties as a continuum rather than distinct neuronal classes. Such a continuum should be possible to define using IF models such as the aeIF model used here.

References

1. Avendaño C, Rausell E, Perez-Aguilar D, and Isorna S. (1988) Organization of the association cortical afferent connections of area 5: a retrograde tracer study in the cat. J. Comp. Neurol. 278: 1-33.
2. Avendaño C, Rausell E and Reinoso-Suarez F. (1985) Thalamic projections to areas 5a and 5b of the parietal cortex in the cat: a retrograde horseradish peroxidase study. J. Neurosci. 5: 1446-1470.
3. Baranyi A., Szente M.B., Woody C.D. (1993a) Electrophysiological characterization of different types of neurons recorded in vivo in the motor cortex of the cat. I. patterns of firing activity and synaptic responses. J. Neurophysiol. 69: 1850-1864.
4. Baranyi A., Szente M.B., Woody C.D. (1993b) Electrophysiological characterization of different types of neurons recorded *in vivo* in the motor cortex of the cat. II. Membrane parameters, action potentials, current-induced voltage responses and electrotonic structures. J. Neurophysiol. 69: 1865-1879.
5. Binzegger T, Douglas RJ and Martin, KAC. (2004) A quantitative map of the circuit of cat primary visual cortex. J. Neurosci. 24: 8441-8453.
6. Borg-Graham L.J., Monier C., Frégnac Y. (1998) Visual input evokes transient and strong shunting inhibition in visual cortical neurons. Nature 393: 369-373.
7. Bourassa J and Deschênes M. (1995) Corticothalamic projections from the primary visual cortex in rats: a single fiber study using biocytin as an anterograde tracer. Neuroscience 66: 253-263.
8. Braitenberg, V. and Schüz, A. (1998) *Cortex: statistics and geometry of neuronal connectivity* (2nd edition). Springer-Verlag, Berlin.
9. Brette R and Gerstner W. (2005) Adaptive exponential integrate-and-fire model as an effective description of neuronal activity. J. Neurophysiol. 94: 3637-3642.
10. Brunel N. (2000) Dynamics of sparsely connected networks of excitatory and inhibitory spiking neurons. J. Comput. Neurosci. 8: 183-208.
11. Cessac, B. (2008) A discrete time neural network model with spiking neurons. Rigorous results on the spontaneous dynamics. J. Math. Biol. 56: 311-345.
12. Cessac, B. and Viéville, T. (2009) On dynamics of integrate-and-fire neural networks with conductance based synapses. Front. Comput. Neurosci. 3: 1.
13. Crutchfield, J.P. and Kaneko, K. (1988) Are attractors relevant to turbulence? Phys. Rev. Lett. 60: 2715-2718.

14. Compte, A., Sanchez-Vives, M.V., McCormick, D.A. and Wang, X.J. (2003) Cellular and network mechanisms of slow oscillatory activity (<1 Hz) and wave propagations in a cortical network model. J. Neurophysiol. 89: 2707-2725.

15. Connors, B.W. and Gutnick, M.J. (1990) Intrinsic Firing patterns of diverse neocortical neurons. Trends Neurosci. 13: 99-104.

16. Contreras D and Steriade M (1995) Cellular basis of EEG slow rhythms: a study of dynamic corticothalamic relationships. J. Neurosci. 15: 604-622.

17. Contreras D., Timofeev I., Steriade M. (1996) Mechanisms of long lasting hyperpolarizations underlying slow sleep oscillations in cat corticothalamic networks. J. Physiol. 494: 251-264.

18. Cossart R, Aronov D, Yuste R. (2003) Attractor dynamics of network UP states in the neocortex. Nature 423: 283-238.

19. de la Peña E and Geijo-Barrientos E. (1996) Laminar organization, morphology and physiological properties of pyramidal neurons that have the low-threshold calcium current in the guinea-pig frontal cortex. J. Neurosci. 16: 5301-5311.

20. Destexhe, A. (2007) High-conductance state. Scholarpedia 2(11): 1341
http://www.scholarpedia.org/article/High-Conductance_state

21. Destexhe A and Contreras D. (2006) Neuronal computations with stochastic network states. Science 314: 85-90.

22. Destexhe A and Paré D. (1999) Impact of network activity on the integrative properties of neocortical pyramidal neurons in vivo. J. Neurophysiol. 81: 1531-1547.

23. Destexhe A, Contreras D and Steriade M. (1998) Mechanisms underlying the synchronizing action of corticothalamic feedback through inhibition of thalamic relay cells. J. Neurophysiol. 79: 999-1016.

24. Destexhe A, Contreras D and Steriade M. (2001) LTS cells in cerebral cortex and their role in generating spike-and-wave oscillations. Neurocomputing 38: 555-563.

25. Destexhe, A., Hughes SW, Rudolph M, Crunelli V. (2007) Are corticothalamic 'up' states fragments of wakefulness? Trends Neurosci. 30: 334-342.

26. Destexhe A, Paré D. (1999) Impact of network activity on the integrative properties of neocortical pyramidal neurons in vivo. J. Neurophysiol. 81: 1531-1547.

27. Destexhe A, Rudolph, M, Paré D (2003) The high-conductance state of neocortical neurons in vivo. Nature Reviews Neurosci. 4: 739-751.

28. Destexhe A, Sejnowski TJ. (2003) Interactions between membrane conductances underlying thalamocortical slow-wave oscillations. Physiol. Reviews 83: 1401-1453.

29. El Boustani, S. and Destexhe, A. (2009) A master equation formalism for macroscopic modeling of asynchronous irregular activity states. Neural Comput. 21: 46-100.

30. El Boustani S, Pospischil M, Rudolph-Lilith M, Destexhe A. (2007) Activated cortical states: experiments, analyses and models. J. Physiol. Paris 101: 99-109.

31. FitzGibbon T, Tevah LV and Jervie-Sefton A. (1995) Connections between the reticular nucleus of the thalamus and pulvinar-lateralis posterior complex: a WGA-HRP study. J. Comp. Neurol. 363: 489-504.

32. Fourcaud-Trocme N, Hansel D, van Vreeswijk C and Brunel N. (2003) How spike generation mechanisms determine the neuronal response to fluctuating inputs. J. Neurosci. 23: 11628-11640.

33. Freund TF, Martin KA, Soltesz I, Somogyi P and Whitteridge D. (1989) Arborisation pattern and postsynaptic targets of physiologically identified thalamocortical afferents in striate cortex of the macaque monkey. J. Comp. Neurol. 289: 315-336.

34. Grenier F, Timofeev I and Steriade M. (1998) Leading role of thalamic over cortical neurons during postinhibitory rebound excitation. Proc. Natl. Acad. Sci. USA 95: 13929-13934.

35. Hines, M.L. and Carnevale, N.T. (1997). The Neuron simulation environment. Neural Computation 9: 1179-1209.

36. Izhikevich EM. (2004) Which model to use for cortical spiking neurons? IEEE Trans. Neural Networks. 15: 1063-1070.

37. Jones, E.G. (1985) *The Thalamus*. Plenum Press, New York.

38. Kim U, Sanches-Vives MV and McCormick DA. (1997) Functional dynamics of GABAergic inhibition in the thalamus. Science 278: 130-134.

39. Kumar A, Schrader S, Aertsen A, Rotter S. (2008) The high-conductance state of cortical networks. Neural Comput. 20: 1-43.

40. Landry P and Deschênes M. (1981) Intracortical arborizations and receptive fields of identified ventrobasal thalamocortical afferents to the primary somatic sensory cortex in the cat. J. Comp. Neurol. 199: 345-371.

41. Lee AK, Manns ID, Sakmann B and Brecht M. (2006) Whole-cell recordings in freely moving rats. Neuron 51: 399-407.

42. Llinás RR. (1988) The intrinsic electrophysiological properties of mammalian neurons: a new insight into CNS function. Science 242: 1654-1664.

43. Matsumura M, Cope T, Fetz EE. (1988) Sustained excitatory synaptic input to motor cortex neurons in awake animals revealed by intracellular recording of membrane potentials. Exp. Brain Res. 70: 463-469.

44. McCormick DA. (1992) Neurotransmitter actions in the thalamus and cerebral cortex and their role in neuromodulation of thalamocortical activity. Prog. Neurobiol. 39: 337-388.

45. Minderhoud JM. (1971) An anatomical study of the efferent connections of the thalamic reticular nucleus. Exp. Brain Res. 112: 435-446.

46. Muller E, Buesing L, Schemmel J, Meier K. (2007) Spike-frequency adapting neural ensembles: beyond mean adaptation and renewal theories. Neural Computation 19: 2958-3010.

47. Paré D, Shink E, Gaudreau H, Destexhe A, Lang EJ. (1998) Impact of spontaneous synaptic activity on the resting properties of cat neocortical neurons in vivo. J. Neurophysiol. 79: 1450-1460.

48. Parga N and Abbott LF. (2007) Network model of spontaneous activity exhibiting synchronous transitions

between up and down States. Front. Neurosci. 1: 57-66.

49. Plenz, D., and Aertsen, A. (1996) Neural dynamics in cortex-striatum co-cultures II - spatiotemporal characteristics of neuronal activity. Neuroscience 70: 893-924.

50. Pospischil, M., Toledo-Rodriguez, M., Monier, C., Piwkowska, Z., Bal, T., Frégnac, Y., Markram, H. and Destexhe, A. (2008) Minimal Hodgkin-Huxley type models for different classes of cortical and thalamic neurons. Biol. Cybernetics 99: 427-441.

51. Rausell E and Jones EG. (1995) Extent of intracortical arborization of thalamocortical axons as a determinant of representational plasticity in monkey somatic sensory cortex. J. Neurosci. 15: 4270-4288.

52. Robertson RT and Cunningham TJ. (1981) Organization of corticothalamic projections from parietal cortex in cat. J. Comp. Neurol. 199: 569-585.

53. Rudolph, M., Pelletier, J-G., Paré, D. and Destexhe, A. (2005) Characterization of synaptic conductances and integrative properties during electrically-induced EEG-activated states in neocortical neurons in vivo. J. Neurophysiol. 94: 2805-2821.

54. Rudolph, M., Pospischil, M., Timofeev, I. and Destexhe, A. (2007) Inhibition determines membrane potential dynamics and controls action potential generation in awake and sleeping cat cortex. J. Neurosci. 27: 5280-5290.

55. Sanchez-Vives, MV and McCormick, DA. (2000) Cellular and network mechanisms of rhythmic recurrent activity in neocortex. Nat. Neurosci. 10: 1027-1034.

56. Sherman, S. M. & Guillery, R. W. (2001) *Exploring the Thalamus.* Academic Press, New York.

57. Smith GD, Cox CL, Sherman M and Rinzel J. (2000). Fourier analysis of sinusoidally driven thalamocortical relay neurons and a minimal integrate-and-fire-or-burst model. J. Neurophysiol. 83: 588-610.

58. Steriade M. (1970) Ascending control of thalamic and cortical responsiveness. Int. Rev. Neurobiol. 12: 87-144.

59. Steriade, M. (2001) Impact of network activities on neuronal properties in corticothalamic systems. J. Neurophysiol. 86: 1-39.

60. Steriade, M. (2003) *Neuronal Substrates of Sleep and Epilepsy*. Cambridge University Press, Cambridge, UK.

61. Steriade M, Amzica F, Nunez A. (1993a) Cholinergic and noradrenergic modulation of the slow ($\sim$0.3 Hz) oscillation in neocortical cells. J Neurophysiol 70: 1384-1400.

62. Steriade M, Deschênes M, Domich L and Mulle C. (1985) Abolition of spindle oscillations in thalamic neurons disconnected from nucleus reticularis thalami. J. Neurophysiol. 54: 1473-1497.

63. Steriade, M., McCarley, R.W. (1990) *Brainstem Control of Wakefulness and Sleep*, Plenum Press, New York.

64. Steriade M, Nunez A and Amzica F. (1993b) Intracellular analysis of relations between the slow ($< 1\ Hz$) neocortical oscillation and other sleep rhythms of the electroencephalogram. J. Neurosci. 13: 3266-3283.

65. Steriade M, Timofeev I, Grenier F. (2001) Natural waking and sleep states: a view from inside neocortical neurons. J. Neurophysiol. 85: 1969-1985.

66. Tél, T. and Lai, Y.-C. (2008) Chaotic transients in spatially extended systems. Physics Rep. 460: 245-275.

67. Timofeev I, Grenier F, Bazhenov M, Sejnowski TJ and Steriade M. (2000) Origin of slow cortical oscillations in deafferented cortical slabs. Cereb. Cortex 10: 1185-1199.

68. Thomson AM and Bannister AP. (2003) Interlaminar connections in the neocortex. Cereb. Cortex 13: 5-14.

69. Updyke BV. (1981) Projections from visual areas of the middle suprasylvian sulcus onto the lateral posterior complex and adjacent thalamic nuclei in cat. J. Comp. Neurol. 201: 477-506.

70. Vogels TP and Abbott LF. (2005) Signal propagation and logic gating in networks of integrate-and-fire neurons. J. Neurosci. 25: 10786-10795.

71. von Krosigk M, Bal T and McCormick, DA. (1993) Cellular mechanisms of a synchronized oscillation in the thalamus. Science 261: 361-364.

72. White EL. (1986) Termination of thalamic afferents in the cerebral cortex. In: *Cerebral Cortex* (Jones EG, Peters A, eds) Vol. 5, pp 271-289. New York: Plenum Press.

73. White EL and Hersch SM. (1982) A quantitative study of thalamocortical and other synapses involving the apical dendrites of corticothalamic cells in mouse SmI cortex. J. Neurocytol. 11: 137-157.

74. Xiang, Z., Huguenard, J.R. and Prince, D.A. (1998) Cholinergic switching within neocortical inhibitory networks. Science 281: 985-988.

75. Zillmer R, Livi R, Politi A and Torcini A. (2006). Desynchronization in diluted neural networks. Phys. Rev. E. 74: 036203.